García-González, D; Rodríguez-Millán, M.; Rusinek, A.; Arias, A. Investigation of mechanical impact behavior of short carbon-fiber-reinforced PEEK composites, in: *Composite Structures, vol. 113, pp. 1116-1126, Dec. 2015*
DOI: https://doi.org/10.1016/j.compstruct.2015.08.028

Investigation of mechanical impact behavior of short carbon-fiber-reinforced PEEK composites

D. Garcia-Gonzalez [a], M. Rodriguez-Millan [b], A. Rusinek [c], A. Arias [a,*]

[a] Department of Continuum Mechanics and Structural Analysis, University Carlos III of Madrid, Avda. de la Universidad 30, 28911 Leganés, Madrid, Spain
[b] Department of Mechanical Engineering, University Carlos III of Madrid, Avda. de la Universidad 30, 28911 Leganés, Madrid, Spain
[c] Laboratory of Mechanics, Biomechanics, Polymers and Structures, National Engineering School of Metz, 1 route d'Ars Laquenexy, CS 65820 57078 METZ Cedex 3, France

ARTICLE INFO

Article history:
Available online 10 August 2015

Keywords:
Short fiber composites
PEEK composites
Impact
Perforation
Brittle failure
Polyether-ether-ketone

ABSTRACT

This paper describes the results of an experimental and numerical investigation of the impact behavior of short carbon fiber reinforced polyether-ether-ketone (SCFR PEEK) composites. The biocompatibility of PEEK and its short fiber composites, their rapid processing by injection molding and suitability for modern imaging have supported technological advances in prosthetic implants used in orthopedic medicine. Surgical implants, including hip and cranial implants, can experience clinically significant impact loading during medical installation and useful life. While the incorporation of short fibers in a thermoplastic matrix can produce significant improvements in stiffness and strength, it can also cause a marked reduction in ductility, making study of their energy absorption capability essential. In this work, the mechanical impact behavior of PEEK composites reinforced with polyacrylonitrile (PAN) short carbon fibers 30% in weight is compared with unfilled PEEK. The perforation tests conducted covered an impact kinetic energy range from 21 J to 131 J, equivalent to the range observed in a fall, the leading cause of hip fractures. Energy absorption capability, damage extension and failure mechanism have been quantified and reported. A numerical modeling that includes homogenization of elastic material and anisotropic damage is presented and validated with experimental data. At all impact energies, SCFR PEEK composites showed a brittle failure and their absorption energy capability decreases drastically in comparison with unfilled PEEK.

1. Introduction

New biocompatible materials and new technologies have made it possible to replace more parts of the human body. Biocompatible purely polymeric materials are showing better properties than metal to use them for prosthetics which are in direct skeletal contact. This is because they require a lower elastic modulus to be structurally compatible [1]. However, purely polymeric materials can present low strength and high ductility. In order to accomplish both low elastic modulus as well as high strength in an efficient manner, polymers are reinforced with fibers [1,2]. The use of short fiber reinforcement reduces the fiber length reinforcing efficiency compared with long fibers, but offers economic and design advantages in biomedical applications with complex geometries, for example injection molding of composite parts with complex shapes.

Short carbon fiber-reinforced PEEK (SCFR PEEK) composites have proven to be a versatile material for use in medical implants due to their suitability for modern imaging technologies, excellent mechanical properties and biocompatibility [3–5]. In addition, SCFR PEEK is a strong and durable composite in the extremely aggressive environment of the human body [2,6]. This family of composites is of particular interest to those manufacturers who develop applications that interact with bone, such as spinal fusion cages and hip prostheses. These prosthetic implants are usually made from metallic alloys with stiffness 10–20 times higher than the adjacent cortical bone leading to problems of mechanical incompatibility [3]. In contrast, the stiffness and strength of PEEK composites can be modified through short carbon fiber filling [2] to match closely the values of bone and achieve optimum mechanical properties for prostheses devices (Fig. 1).

Although incorporating short carbon fibers in a PEEK thermoplastic matrix produces an improvement of its biomechanical properties, it can also cause a marked reduction in ductility and associated embrittlement of the material [7,8]. This deterioration in impact behavior can limit the application of prosthetic devices. Bones and potential prosthetic devices provide structural support for the body and they must be able to absorb enough energy above its ultimate strength without showing fracture [2]. Therefore, it is essential to study the effect of reduced ductility in order to

* Corresponding author. Tel.: +34 916249161.
E-mail address: aariash@ing.uc3m.es (A. Arias).

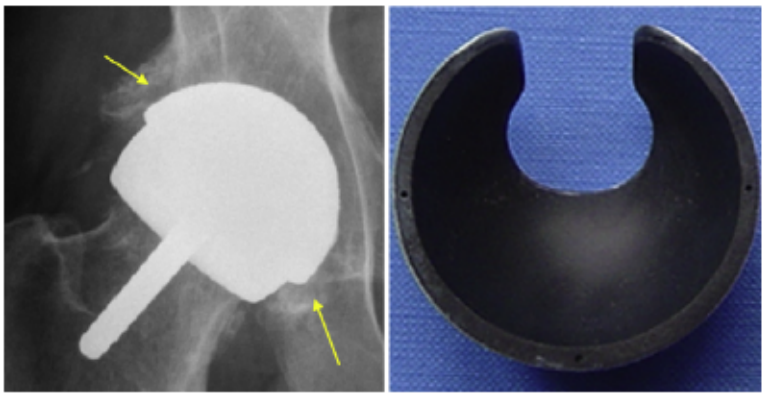

Fig. 1. Fixation of acetabular prosthesis of CF30 short fiber PEEK [9].

determine the levels of energy absorption of prostheses, such as cranial implants and hip systems [9], in dynamic conditions. Investigation of mechanical impact behavior of medical implants needs to include levels of dynamic loading commonly generated in a fall or accident.

Mechanical impact process is a complex problem that includes dynamic behavior, fracture, damage, contact and friction [10,11]. For PEEK composites, interesting thermo-mechanical phenomena have been reported associated with high strain rate in dynamic process: changes in ductile–brittle transition, toughness, fracture energy and failure mechanisms [12,13]. Experimental observations of some authors have shown no significant influence on mechanical properties of short fiber reinforced thermoplastic composite under low strain rates demonstrating elasto-plastic behavior [14]. For high strain rates experimental stress–strain curves showed an elasto-viscoplastic behavior although this dependence is neglectable for temperatures near to glass transition [15,16]. Moreover, especially in dynamic conditions, the mechanical response of such composite material is highly sensitive to the short fiber orientation. In this regard, injection molding is the widely used process for the production of SCFR PEEK composites with complex shapes. The orientation of the fibers induces heterogeneity throughout the material, making the prediction of its behavior and ruptures a challenging task.

The impact behavior of SCFR PEEK composites has not been deeply studied in terms of kinetic energy absorption and failure under impact loading, and perforation tests have not been reported in the scientific literature. In this work, a study in terms of energy absorbed has been experimentally developed in order to analyze the mechanical impact behavior of short carbon fiber reinforced PEEK composites and unfilled PEEK biomaterials which are frequently used for medical applications. The perforation experiment covered an impact kinetic energy range from 21 J to 131 J, equivalent to the range observed in a fall of a person. C-Scan and scanning electron microscope (SEM) inspection tests have been conducted to reach a better understanding of damage extension and failure mechanisms. Additionally, in order to predict the response of material a new approach for modeling the behavior of SCFR PEEK composites has been developed. The model includes homogenization of elastic material and anisotropic damage. A validation of the predictions against experimental data is conducted for short carbon fiber PEEK composite.

2. Material

Commercial plates of PEEK composites reinforced with PAN short carbon fibers 30% in weight, named CF30 PEEK, and unfilled PEEK plates of general purpose grade were purchased measuring $130 \times 130 \times 3\ mm^3$. Both materials are produced with injection molding technology. Carbon fiber is currently the most widely used fibrous reinforcing agent for PEEK based composites [17] due to the strong interfacial interaction between short carbon fibers and PEEK matrix. The interfacial strength between short carbon fibers and PEEK polymer is higher than other known combinations of fibers and thermoplastic matrices [3,7,18], and on average, at least an order of magnitude stronger than that between carbon fibers and ultra-high-molecular-weight polyethylene (UHMWPE) polymers [15,18]. This supports the use of PEEK in preference to UHMWPE in combination with carbon fibers for applications such as bearing medical surfaces. For CF30 PEEK, the diameter and length of PAN carbon fiber were 7 μm and 200 μm respectively. The percentage of 30% carbon fiber in weight (23.5% in volume) of CF30 PEEK provides optimum rigidity and load bearing capability. Due to its biocompatibility and high strength, CF30 PEEK has been successfully used in humeral plates, cranial implants and composite acetabular inserts in hip replacement procedures [2,5,19]. The mechanical properties of PEEK and CF30 PEEK composite are shown in Table 1 [20], supported by data published by authors [21]. Addition of short fiber into PEEK matrix increases the low elastic modulus from 3.6 GPa for neat PEEK to 24 GPa for SCFR PEEK and it doubles the failure strength value. Failure strength in this paper refers to ultimate tensile strength or yield stress, according to which was reached first in tensile testing [7].

2.1. Mechanical characterization of SCFR PEEK composite

One inherent problem in processing short fiber reinforced thermoplastics (SFRTPs) by flow molding techniques is that the fibers will tend to become aligned during the flow process, inducing anisotropic material properties. To investigate the effect of orientation on the mechanical behavior, tensile and compressive tests of

Table 1
Mechanical properties of PEEK and CF30 PEEK composite [20,21].

	SCFR PEEK composite (CF30)	Unfilled PEEK
Elastic Modulus (GPa)	24	3.6
Poisson's ratio	0.385	0.38
Density (kg/m^3)	1400	1300
Yield stress (MPa)	–	107
Tensile strength (MPa)	214	95
Elongation at break (%)	2.0	40.0
Charpy impact strength (kJ/m^2)	6.50	7.0
Glass transition temperature (K)	416	416
Melt transition temperature (K)	610	616

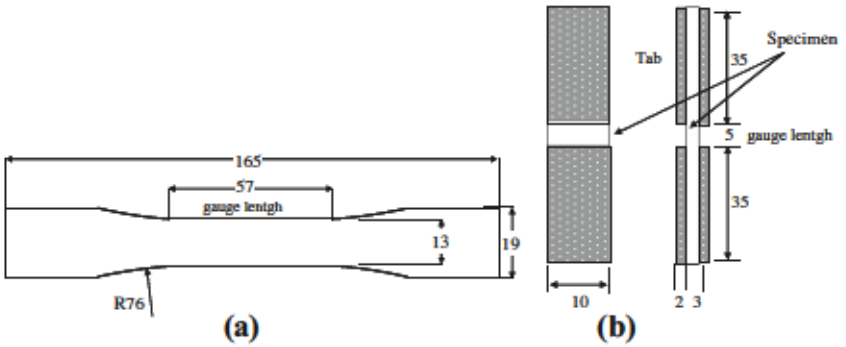

Fig. 2. Geometry of specimen for tensile test ASTM D-638 and compression test ASTM D-695 (dimensions in mm).

Table 2
Mechanical properties of SCFR PEEK in both IFD longitudinal and transversal material directions.

Mechanical properties	SCFR PEEK composite (CF30), this work		SCFR PEEK composite (CF30) [22]
	Transversal	Longitudinal	Longitudinal
Tensile strength (MPa)	148	214	220.8
Compressive strength (MPa)	174	239	246.2
Tensile elastic modulus (GPa)	12.6	24	23.2
Compressive elastic modulus (GPa)	15	44	43.5
Poisson's ratio (−)	0.38	0.38	0.38
Elongation at break (%)	1.9	2.0	1.8

injection molded specimens were conducted using a servo-hydraulic testing machine INSTROM 8516 under displacement control at 1 mm min^{-1}. Tensile and compressive samples were machined on the ASTM D-638 recommendations, Fig. 2a, and ASTM D-695, Fig. 2b. An INSTROM 2620 extensometer and HBM strain gages were used to increase the accuracy of the strain data. Young's modulus (E) and failure strain and their respective strains were determined as the mean value of at least eight specimens and results are shown in Table 2. Fig. 3 shows stress–strain curves of CF30 PEEK composite, in agreement with data of the works published by Sarasua and Remiro [8] and Lee [22]. Fig. 4 shows the stress–strain curves of tensile and compression tests for CF30 PEEK composite in both IFD longitudinal and transverse directions. These experimental results show that tensile strength, compressive strength and failure of CF30 PEEK composite is dependent on material direction. Longitudinal values are higher for both tensile strength and compressive strength. Short fibers are mainly aligned in the injection flow direction (IFD), providing higher longitudinally than in the transverse direction. In addition, the results showed an enhanced behavior under compressive loading than tensile loading (Table 2). Specimens machined in the flow direction showed tensile and compressive strength approximately 40% lower than specimens machined transverse to the flow direction. It was observed no significant influence of strain rate on stress–strain curves in the range from 10^{-4} s^{-1} to 10^{-1} s^{-1}, in agreement with the works of Kammount et al. [15].

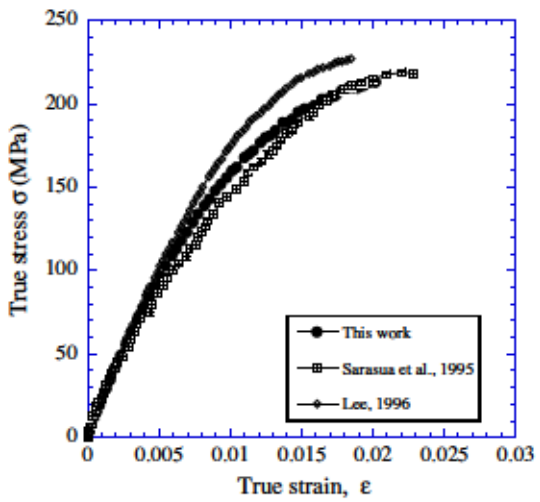

Fig. 3. Comparison of stress–strain of CF 30 PEEK composite given by experimental data of this work and experimental data of works of Sarasua and Remiro [8] and Lee [22].

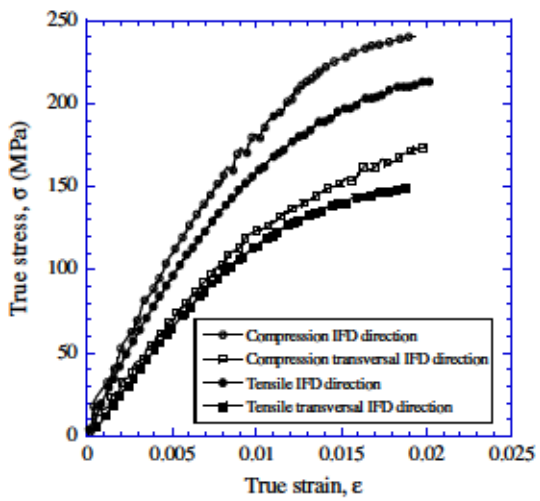

Fig. 4. Mechanical behavior of CF 30 PEEK composite under compression and tension for specimen machined in the IFD longitudinal direction and transverse direction.

2.2. Crystallinity

Mechanical properties of PEEK materials are influenced by the degree of crystallinity. Several authors have shown that increasing the degree of crystallinity can increase elastic modulus and yield strength while decreasing fracture toughness [12,23]. From differential scanning calorimetry (DSC) a degree of crystallinity of 30 ± 2% was calculated for PEEK and 32 ± 2% for CF30 PEEK integrating the melt endotherm [24]. The results of DSC testing did not show significant differences in the ability of matrix to crystallize between unreinforced PEEK and CF30 PEEK. This finding is in agreement with data reported by Sarasua and Remiro [8].

2.3. Strain rate and temperature sensitivity

The effect of strain rate and temperature on mechanical behavior of short fiber thermoplastic composites has been reported in the literature [13,25,26]. Wang et al. [25] showed that short fiber thermoplastic composite is a strain rate and temperature dependent material. Both the elastic modulus and tensile strength of the composite increased with strain rate and decreased with temperature. However, for temperatures near to glass transition the stress–strain curves of composites are not sensitive to strain rates with less than 2% change in elastic modulus are less than 2% and less than 10% change in tensile strength. The values of impact fracture toughness of short fiber reinforced PEEK is similar to unfilled PEEK at room temperature and quasi-static conditions [13,26]. Toughness of short fiber reinforced PEEK and unfilled PEEK decrease with strain rate but this effect is inverted if high temperatures near glass transition are reached due to adiabatic effects associated with the impact process.

3. Experimental impact testing

3.1. Hip and skull fracture energy

Hip fractures, the leading morbidity resulting from falls, constitute a major and growing socioeconomic problem in health care [27,28]. Since PEEK composites studied in this work are employed for hip replacements [9,25], the impact energy generated in a fall has been used as the reference level. Estimating the available energy W_{hip} just before impact by kinetic energy E_K, it is possible to approximate the impact energy involved in a fall affecting the hip. The average value for vertical hip impact velocity has been determined as 2.75 m/s [29]. For a person of 66 kg, taking the effective mass corresponding to the hip zone as one sixth of the total body weight (overestimated), the maximum impact energy affecting the hip corresponding to an accidental fall is equal to $W_{hip}^{fracture} = 42$ J. Head protection measures and proposed skull fracture criteria typically include the energy absorbed up to the point of skull fracture [30,31]. This reference skull fracture energy ranges from 21.1 J to 40.5 J. Therefore, in this study, the kinetic energy range has been $21.0\,\text{J} \leqslant E_K \leqslant 131.0\,\text{J}$ including the range of hip and skull fracture impact energy and incorporating a higher upper limit. For this proposal, perforation tests using rigid spheres were conducted on plates of CF30 PEEK and unfilled PEEK.

3.2. Experimental setup

The set-up used was a gas gun capable of shooting a rigid spherical projectile with a mass of $m_p = 1.3$ g and a diameter of $\phi_p = 6.82$ mm. This experimental device uses helium up to pressures of 200 bars to impel the projectile. The initial impact velocity V_0 was in a range of $170\ \text{m/s} \leqslant V_0 \leqslant 450\ \text{m/s}$. In order to measure the impact and the residual velocity, a high speed video camera (Photron Ultima APX-RS) was used. Since the exposure time was very short, 10 μs, a 1200 W HMI lamp was used to ensure adequate lighting. The camera was configured to obtain 36,000 frames per second (fps). Plates of dimensions of CF30 PEEK and unfilled PEEK were tested. Plates of Ti6Al7Nb and Ti6Al4V titanium alloys were also studied to allow comparison between the CF30 PEEK, unfilled PEEK, and alloys used in biomedical applications. The thickness of each plate was selected to obtain comparable areal density [21,32], a parameter frequently used to optimize impact protection (Table 3). The thickness of both titanium alloys was set at $t = 1$ mm providing a representative comparison. Due to the boundary conditions used to avoid sliding and to ensure correct clamping of the specimen, the size of the active part of all the plates were reduced to $100 \times 100\ \text{mm}^2$, Fig. 5.

Table 3
Biomaterials considered for impact testing.

Material	Dimensions (mm^3)	Mass (g)	Areal density (kg/m^2)
CF30 PEEK composite	130 × 130 × 3	70.2	4.1
Unfilled PEEK	130 × 130 × 3	65.5	3.9
Ti6Al4V	130 × 130 × 1	78.5	4.6
Ti6Al7Nb	130 × 130 × 1	79.4	4.7

4. Modeling behavior of PEEK composite

Accurate description of the SCFR-PEEK mechanical impact behavior needs to take into account the preferential alignment of fibers in the injection molding direction, IFD [8,33]. The results of experimental testing in this study (Fig. 4), consistent with other studies [7,8], have demonstrated that fiber alignment affects the mechanical properties of SCFR-PEEK. Model parameters were identified based on the experimental results of compressive tests, using the methodology reported for PEEK polymers [21] and assuming brittle linear elastic behavior in compression [34–36].

4.1. Linear elastic behavior

The mechanical response of the material to stress state is the result of both the matrix and the fibers contributions to that response. The constitutive modelling of thermoplastics reinforced with short carbon fibers has been widely investigated and constitutive models relying on two main approaches have been developed. The first approach is based on the consideration of an assembly of the damageable elastoplastic matrix material and one-dimensional linear elastic fiber media. These models treat separately the matrix response and the fibers response following any variation of the composite materials mixture rule [37–39]. The second approach is based on the homogenization of the elastic composite behavior by defining a homogenized stiffness tensor from the matrix and the reinforcement fibers [15,40]. Amongst those using models based on homogenization, some authors allow for linear elastic behavior [40], while others include rate-dependency in the elastic behavior [15]. The model described in this work follows a simple homogenization scheme based on the Voigt mixing rule algorithm. In order to get a more clear understanding of the formulation proposed in this model, all the tensor components are written in bold style and scalar components in normal style. This model assumes uniform strain in the two phases and defines the homogenized stiffness tensor $\boldsymbol{C}_{comp}$ as:

$$\boldsymbol{C}_{comp} = \left[(1-\phi_m)\cdot \boldsymbol{C}_f + \phi_m \cdot \boldsymbol{C}_m\right] \tag{1}$$

where ϕ_m is the matrix material in concentration and $\boldsymbol{C}_f$ and $\boldsymbol{C}_m$ are the fiber stiffness tensor and the matrix stiffness tensor respectively. Thus, the homogenized stress $\boldsymbol{\sigma}_{comp}$ can be written as:

$$\boldsymbol{\sigma}_{comp} = \boldsymbol{C}_{comp} \cdot \boldsymbol{\varepsilon}_{comp} \tag{2}$$

where $\boldsymbol{\varepsilon}_{comp}$ is the homogenized strain, the macro strain. In this way, the SCFR-PEEK behavior has been defined as a linear anisotropic elastic material, with a mechanical response that is completely determined by the homogenized stiffness tensor depending on the following elastic parameters: Young's modulus in direction of IFD, $E_{longitudinal} = 44$ GPa; Young's modulus in transverse direction to the IFD, $E_{transverse} = 44$ GPa; longitudinal shear modulus $G_{12} = 5.7$ GPa; and Poisson's coefficient $\nu_{12} = 0.385$. The transverse shear modulus G_{23} and G_{13} have been obtained from the theory of Hill and Hashin [41,42]. These elastic parameters are all in

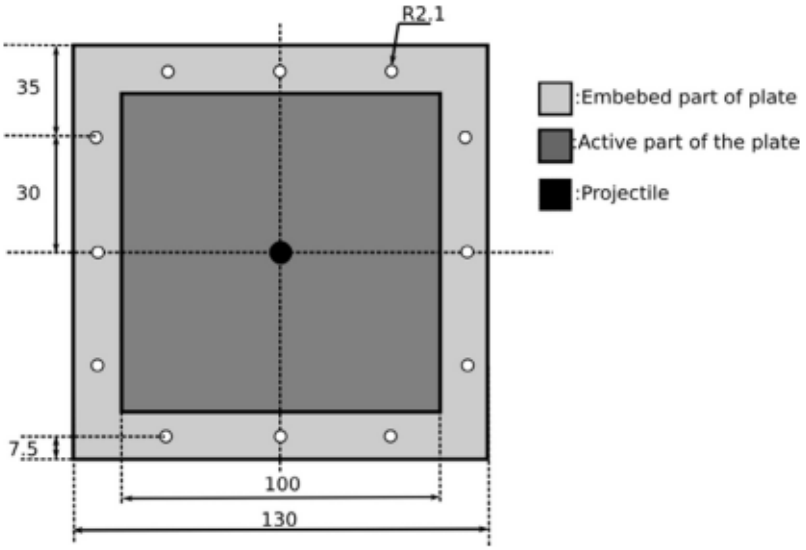

Fig. 5. Geometry of plate specimen and boundary conditions (dimensions in mm).

agreement with the Halpin-Tsai equations [43] and the experimental data reported by Lee [22].

4.2. Damage initiation criterion

Due to good adhesion between short carbon fibers and matrix, the failure of PEEK composite is reported as cohesive [2,8,18]. This failure is also dependent on material direction, with both tensile and compressive strength varying with direction. Short fibers are mainly aligned along the injection molding direction, IFD. This provides higher strength in IFD direction than in the transverse direction under usual loading conditions. As outlined in 2.1, results show an enhanced mechanical behavior under compressive loading than under tensile loading. With regard to strength, longitudinal values are higher than transverse values both in tension and compression.

Based on these observations, it was defined as a Tsai-Hill failure criterion in order to determine damage initiation. Some authors have employed this failure criterion to define the material behavior of short-fiber reinforced thermoplastics produced by injection molding [15,44]. Kammoun et al. [15], in determining Tsai-Hill criterion, assumed plane stress conditions in laminated composites with aligned, continuous fibers inside individual thin plies. This has been shown to be a valid assumption as injection molded sheets show quasi in-plane orientation distribution of the fibers. However, Kammoun et al. [15] have suggested, due to the limitations of this assumption, the selected failure criteria would only reveal approximate trends and they recommend the development of more appropriate 3D failure criterion. Following their recommendations a Tsai-Hill failure criterion has been programmed in a VUMAT subroutine in order to establish a damage initiation criterion considering the 3D formulation, Eq. (3).

$$\frac{\sigma_{11}^2}{X^2}+\frac{\sigma_{22}^2}{Y^2}+\frac{\sigma_{33}^2}{Z^2}-\left(\frac{1}{X^2}+\frac{1}{Y^2}+\frac{1}{Z^2}\right)\cdot\sigma_{11}\sigma_{22}-\left(\frac{1}{X^2}+\frac{1}{Y^2}+\frac{1}{Z^2}\right)\cdot\sigma_{11}\sigma_{33}-\left(\frac{1}{X^2}+\frac{1}{Y^2}+\frac{1}{Z^2}\right)\cdot\sigma_{22}\sigma_{33}+\frac{\tau_{12}^2}{S_{12}^2}+\frac{\tau_{13}^2}{S_{13}^2}+\frac{\tau_{23}^2}{S_{23}^2}=1 \quad (3)$$

where the normal strengths in the IFD in traction and compression were defined as $X_t = 214$ MPa and $X_c = 239$ MPa; the normal strengths in the transverse direction to the IFD (Y and Z) in traction and compression were defined as $Y_t = Z_t = 214$ MPa and $Y_c = Z_c = 239$ MPa; and the shear strengths were defined as $S_{ij} = 109.9$ MPa. These data is in agreement with the experimental observations of the anisotropic behavior presented by the elastic composite material considered in this study.

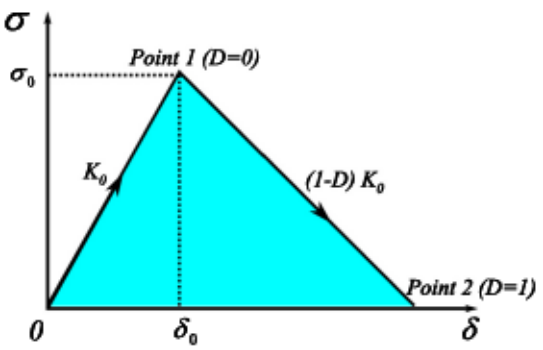

Fig. 6. Scheme of constitutive model implemented.

4.3. Damage evolution

In order to define the material behavior once the damage has been initiated, a damage evolution model has been defined to describe the degradation rate of the material strength after the initiation criterion is satisfied. The stress–strain curve exhibits a linear elastic stage until the load increases to the critical value at *Point 1*. This point is reached when the damage initiation criteria, in our case Tsai-Hill criterion, is satisfied. Following the scheme shown in Fig. 6, degeneration of the load carrying capacity after damage initiation occurs from Point 1 to Point 2. The value of the damage parameter D goes from 0 (indicating there is no damage, at Point (1) to 1 (indicating a complete failure of the material, reached in Point (2). This parameter is used in combination with the stiffness coefficients to calculate the stiffness coefficient in damage evolution, defined as:

$$\boldsymbol{K} = (1-D)\boldsymbol{K_o} \quad (4)$$

where $\boldsymbol{K_o}$ is the stiffness coefficient of intact material.

In this work, a dependency has been observed between the degradation of the material and the increase in strain once the

failure starts. Base on this observation, the damage parameter D has been defined as:

$$D(\bar{\varepsilon}) = \Sigma \Delta\bar{\varepsilon} \cdot \psi \tag{5}$$

where $\Delta\bar{\varepsilon}$ is the strain increment in each time increment and ψ is a material constant controlling the material degradation due to the total strain accumulated once the damage initiation criterion is satisfied.

To avoid sudden changes in the stiffness of the finite elements when damage occurs leading to instability problems and lack of convergence during the simulation, the stress components were corrected using a smooth transition, Eq. (6).

$$\sigma_{ij}^{*} = \sigma_{ij}\left[1 - \frac{2 - e^{s\left(D_i - \frac{1}{2}\right)}}{2 - e^{\frac{s}{2}}}\right] \tag{6}$$

where σ_{ij}^{*} and σ_{ij} are the stress before and after the correction, D_i is the corresponding damage parameter, and s is the variable which controls the slope of the stress decay when the damage is close to 1. According to recommendations a value $s = 30$ was adopted [45].

5. Numerical model

A Lagrangian 3D finite element model for the simulation of the perforation process was developed in ABAQUS/Explicit [46]. The geometry of plates is equal to the active area of the experimental tests specimens (100×100 mm) with a value of thickness equal to 3 mm for short fiber PEEK composite (Table 3). The fully 3D configuration allows the model to describe the radial cracking and the shear failure mode that characterize the perforation of plates by spherical projectiles [47]. The target mesh developed is shown in Fig. 7, where twelve elements were placed across the thickness of the target. This is in agreement with the recommendations reported [46], where it is suggested that at least four elements should be used through the thickness when modeling any structures carrying bending loads. The mesh presents radial symmetry to avoid spurious generation of cracks. The mesh is split into three different zones. The zone directly affected by the impact has been meshed with 32,400 tri-linear elements with reduced integration (C3D8R in ABAQUS notation). In order to reduce the computational time, a transition zone is defined beyond the zone directly affected by the impact using 48,000 elements. After the transition zone, the mesh is defined using C3D8R elements until reaching the perimeter of the target. This optimum configuration has been obtained from a convergence study using different mesh densities. Since the experimental observations revealed absence of erosion on the projectile-surface after the impact (the projectile was not deformed plastically in any test), the projectile has been defined as rigid body. This enables a reduction in the computational time required for the simulations. A constant friction coefficient value $\mu = 0.27$ [27,48] has been used to define the contact projectile/plate. The potential dependence of the friction coefficient on the temperature and the sliding velocity is not taken into account. The constant value used for the friction coefficient is based on the assumption of a constant pressure along the projectile-plate contact zone. The authors confirmed this hypothesis by FE analysis of different projectile-target configurations [49]. The impact velocities covered with the numerical simulations are those covered during the normal impact experiments.

6. Results and discussion

6.1. Energy absorption of SCFR PEEK composite

Firstly, the experimental results of impact velocities are analyzed. Fig. 8a shows the residual velocity versus impact velocity ($V_r - V_0$) curves obtained for both materials tested, SCFR PEEK composite and unfilled PEEK. Fig. 8a also shows the experimental results for results for titanium alloys Ti6Al4V and Ti6Al7Nb, materials commonly used in biomedical applications. The ballistic limit V_{bl} is the maximum value of the initial impact velocity V_0 which induces a residual velocity V_r equal to zero. The ballistic limit of PEEK unfilled, $V_{bl}^{PEEK} \approx 265$ m/s, was found to be greater than that corresponding to the SCFR-PEEK, $V_{bl}^{SCFR-PEEK} \approx 177$ m/s, and also greater than the ballistic limit of both titanium alloys considered, $V_{bl}^{Ti6Al4V} \approx 232$ m/s and $V_{bl}^{Ti6Al7Nb} \approx 237$ m/s. The results shown in Fig. 8a have fitted via the expression proposed by Recht and Ipson [50]:

$$V_r = \left(V_0^k - V_{bl}^k\right)^{1/k} \tag{7}$$

where k is a fitting parameter. The values of k determined are $k = 1.8$ for SCFR-PEEK composite, $k = 1.9$ for unfilled PEEK, $k = 2$ for Ti6Al4V and $k = 1.8$ for Ti6Al7Nb. The residual velocity of PEEK unfilled plates within the range of impact velocities tested is lower than SCFR-PEEK composite and both titanium alloys. Based on the measurements described previously, it is possible to estimate the energy absorption W of composite under dynamic impact by Eq. (8) and the minimum energy to perforation, $W_{perforation}$, Eq. (9).

$$W = \frac{1}{2} m_p \left(V_0^2 - V_r^2\right) \tag{8}$$

$$W_{perforation} = \frac{1}{2} m_p V_{bl}^2 \tag{9}$$

Fig. 8b shows the kinetic energy of the projectile converted into energy absorbed W of composite. For all materials tested W increases with initial velocity. This tendency is in agreement with experimental results published in the literature for spherical noses of projectile [10,21]. Comparing the values obtained, it is observed that PEEK unfilled can absorb enough energy to avoid hip and skull

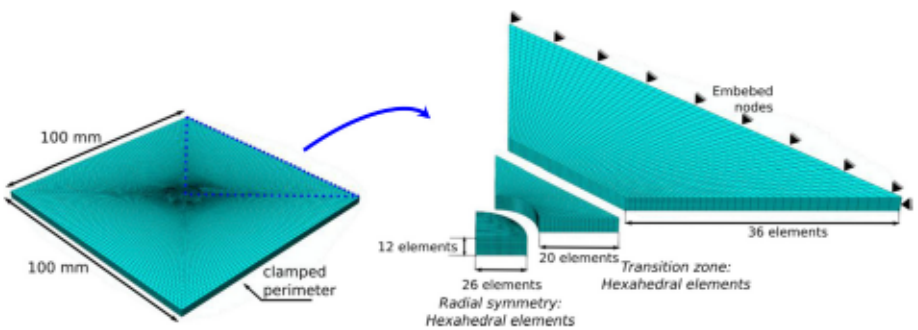

Fig. 7. Numerical configuration used in the simulations.

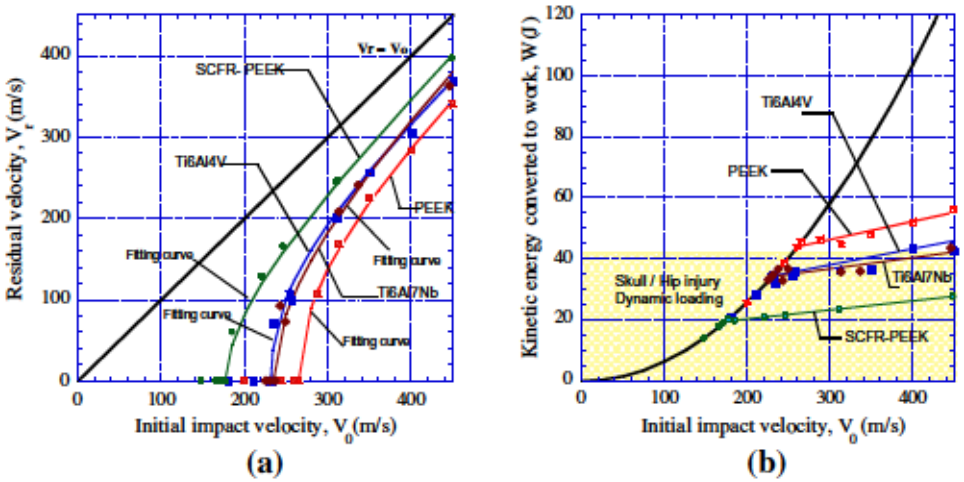

Fig. 8. (a) Residual velocity V_r versus impact velocity V_0, comparison between PEEK composites and titanium alloys; (b) Energy absorbed by the plate W versus impact velocity V_0, comparison between PEEK composites and titanium alloys.

injuries independent of the impact velocity, Fig. 8b.The reference used for comparison is the maximum hip fracture energy, $E_{hip}^{fracture} = 42$ J, reported in [31]. The values of perforation energy are respectively $W_{perforation}^{PEEK} = 45.6$ J, $W_{perforation}^{SCFR-PEEK} = 20.4$ J, $W_{perforation}^{Ti6Al4V} = 35$ J and $W_{perforation}^{Ti6Al7Nb} = 36.5$ J. Moreover, over the full range of impact velocities, PEEK material is more efficient in energy absorption compared to both SCFR-PEEK with a medium ratio of $R = 1.85$ and titanium alloys with a medium ratio of $R = 1.26$, Fig. 9. In addition, SCFR-PEEK composites do not have the capacity to absorb all energy without fracture for values higher than 20.4 J. At high strain rate, SCFR-PEEK composites increase its brittleness with associated reduction of toughness [26]. The lack of energy dissipation by plastic deformation of the matrix increases the impact energy transferred locally to the composite which can generate fractures and perforation.

6.2. *Failure mode of SCFR PEEK composite*

Fracture in short fiber thermoplastic composite takes place progressively by the succession and overlapping of several complex failure mechanisms. In these composites failure occurs as the result of a variety of complex damage mechanisms such as fiber cracking, fiber debonding and pull-out, plastic localization and ductile fracture (void growth and coalescence) in the matrix [15]. Figs. 10–13 illustrate the final stage of the impact process for different initial impact velocities and both materials tested. The failure mode of SCFR PEEK composite is clearly different from that observed in unfilled PEEK. While PEEK unfilled behaves in a ductile manner, when short fibers are added, the SCFR PEEK shows a marked change to brittle behavior resulting in a considerable loss in energy absorption capability. For SCFR PEEK composite and on the front and rear, Fig. 10a and b respectively, damage was a combination of localized penetration in local impact zone and four long brittle cracks in radial directions and deep of thickness size of specimen. This observation demonstrates a key failure mechanism based on a cohesive failure mode due to insufficient matrix shear strength in impact conditions. For unfilled *PEEK matrix* and on the front and rear surfaces, Fig. 10c and d respectively, damage was localized and ductile for two consecutive impacts showing multi-hip capatibility for impact absorption energy [21].

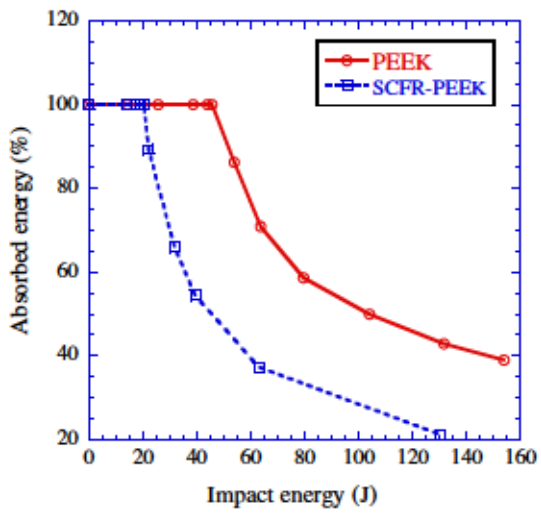

Fig. 9. Percentage of absorption energy of SCFR PEEK and unfilled PEEK versus impact energy.

For a better understanding of the impact processes in composite materials [51], two different regimes can be considered: impact velocities below and above ballistic limit V_{bl}. When the impact velocity is not high enough to perforate the composite, below ballistic limit, it is assumed that the plate absorbs all the kinetic energy of the projectile mainly in form of matrix cracking damage, Fig 11a. Low velocity impact involves a long contact time between the impactor and the target, which produces damage in some points far from the contact region (global structure deformation). For this reason, the matrix cracking usually observed due to low-velocity impact, occurs parallel to the fibers of brittle composite. However, if the impact velocity of the projectile is high enough to perforate the plate, the energy absorbed by the composite is only the difference between the initial and the residual kinetic energy of the projectile, Fig 11b and c. In this case, some part of the energy is absorbed by fiber cracking, fiber pull-out and local matrix failure (to create the plug) and some other is used to accelerate the plug (linear momentum transfer) from rest of the projectile residual velocity. Here the damage extension is much greater compared to the previous velocity analyzed. Finally, at very high velocities the damage induced by the projectile is much more localized around the impact point; projectile pushes a plug out of the target approximately equal in diameter to that the projectile; this means that the damaged area is smaller than at lower velocities (above ballistic limit).

At impact velocities above the ballistic limit, a spalling process of the material was observed around the hole created by the penetration of the projectile and the plug ejected during the impact is

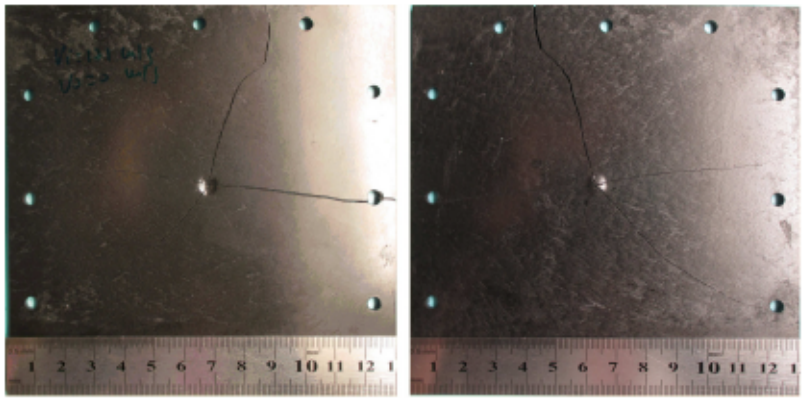

(a) *Impact Energy 19.01 J. V_0=171 m/s. V_r =0 m/s. Front surface*

(b) *Impact Energy 19.01 J. V_0=171 m/s. V_r =0 m/s. Rear surface*

(c) *$V_0(1)$=260 m/s; $V_0(2)$=244 m/s; V_r=0 m/s. Front surface*

(d) *$V_0(1)$=260 m/s; $V_0(2)$=244 m/s; V_r=0 m/s. Rear surface*

Fig. 10. Final stage of the perforation process of SCFR PEEK and unfilled PEEK for different impact velocities (front and rear surfaces of plates).

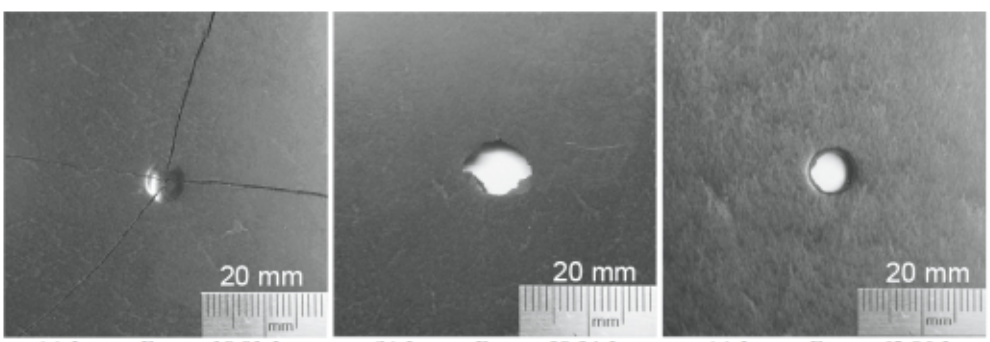

(a) *Impact Energy 19.01 J. V_0=171 m/s. V_r=0 m/s*

(b) *Impact Energy 39.34 J. V_0=246 m/s. V_r=166 m/s.*

(c) *Impact Energy 62.86 J. V_0=311 m/s. V_r=246 m/s.*

Fig. 11. Final stage of the perforation process of SCFR PEEK composite for different impact velocities below ballistic limit and above ballistic limit.

supposed to approximate a truncated cone. On the rear surface (Figs. 12 and 13) the damage was higher compared to the front surface one. This can be attributed to the global deformation influence (along with the local damage) that causes the damage of the larger area on the rear surface. Moreover, radial cracks are observed in the rear surface. This type of radial fracture is common in materials where the tensile strength is lower than the compressive strength as it has been determined for SCFR composite in Section 2.

As experimental complementary technique C-Scan technique was used to measure the damaged area; this non-destructive inspection method allows performing an accurate quantification of the damage extent based on the elastic wave's attenuation passing through discontinuities. It is corroborated that the extension of damaged area is limited to macroscopic observations: spalling around the hole created by the projectile penetration and radial cracks, Fig. 14. The damaged area decreases with impact velocity up to a surface equivalent to the perfect hole of the projectile at high velocities. Moreover, using SEM photo, Fig. 15a and b, it is possible to note a global brittle behavior characterized by: SCF/PEEK interfaces (I), micro-cracking and matrix deformation (II), fiber pull-out (III) and fiber breakage (IV). Observations of fracture surfaces revealed the existence of a high amount of matrix adhered

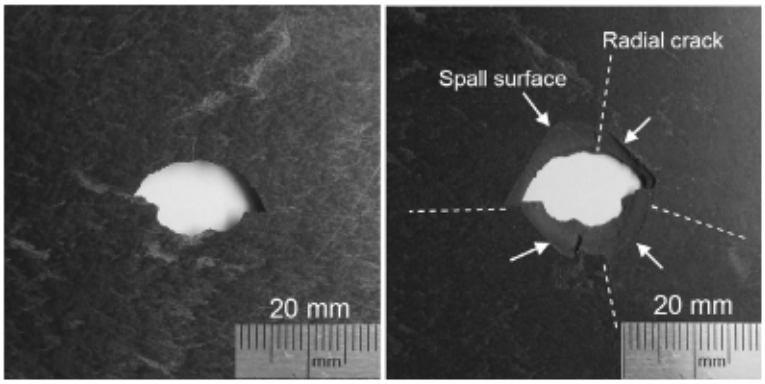

Fig. 12. Damage in front and rear surface of plates of SCRF PEEK composite impacted at V_0 = 221 m/s.

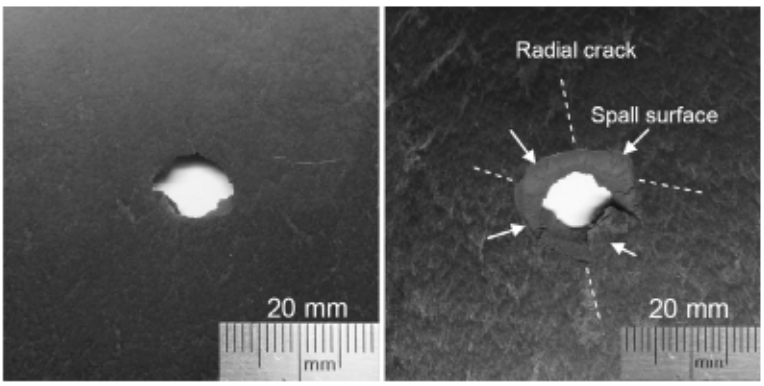

Fig. 13. Damage in front and rear surface of plates of SCRF PEEK composite impacted at V_0 = 246 m/s.

to fiber surfaces, characteristic of the high interfacial strength between short carbon fibers and PEEK polymer [8,18]. There are not "clean fibers" and all fibers show some adhering of PEEK polymer [3]. Long pull-out lengths are observed in impact at low velocities, Fig. 15a, due to a higher contact time between projectile and plate and more energy absorption of composite, Fig. 9. Fig. 15a and b show also that debonding is proved to initiate preferentially at fiber tips due to stress concentration in impact zone, followed by of a separation of interface, formation of microvoids and their propagation along fiber sides up to cracks propagation in the matrix [52]. Fiber breakage is minority, Fig. 15a in agreement with results of work reported by Notta-Cuvier et al. [38]. Thus, it is confirmed that fiber breakage rarely plays a leading role in the failure of injection moulded SFRC since fibers have an initial length higher than the critical value.

6.3. Numerical simulations

A good correlation was found between experimental and numerical results, with a maximum error less than 10%, which demonstrates that the models used in this study faithfully reproduce the impact behavior of SFC PEEK, Fig. 16a. From numerical predictions simulations, the values of damage area have been obtained showing a decrease with impact energy. These numerical predictions of the damaged area were estimated in terms of the damage variable $D(\bar{\varepsilon})$, Eq. (5), defined as a state variable in a

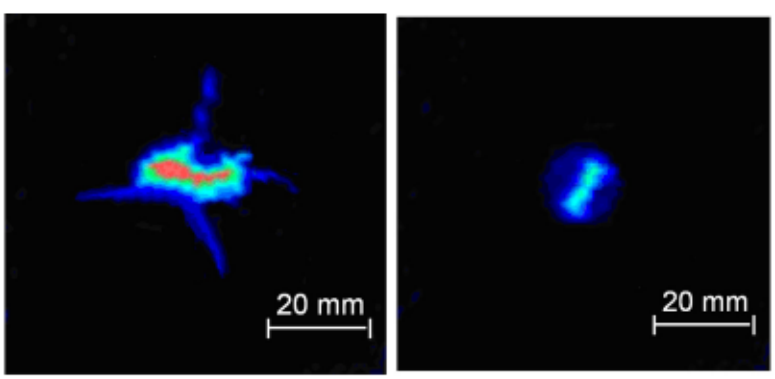

Fig. 14. C-Scan image of impacted SCRF PEEK composite plates: (a) Impact velocity, V_0 = 221 m/s; (b) Impact velocity, V_0 = 311 m/s.

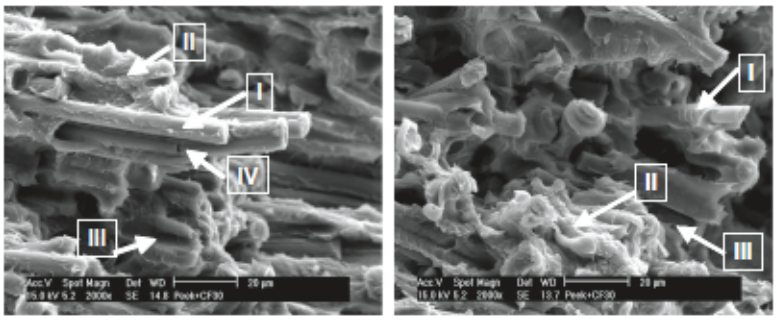

Fig. 15. Scanning electron micrograph of the fracture surface of impacted SCRF PEEK composite: (a) Impact velocity, V_0 = 221 m/s; (b) Impact velocity, V_0 = 246 m/s.

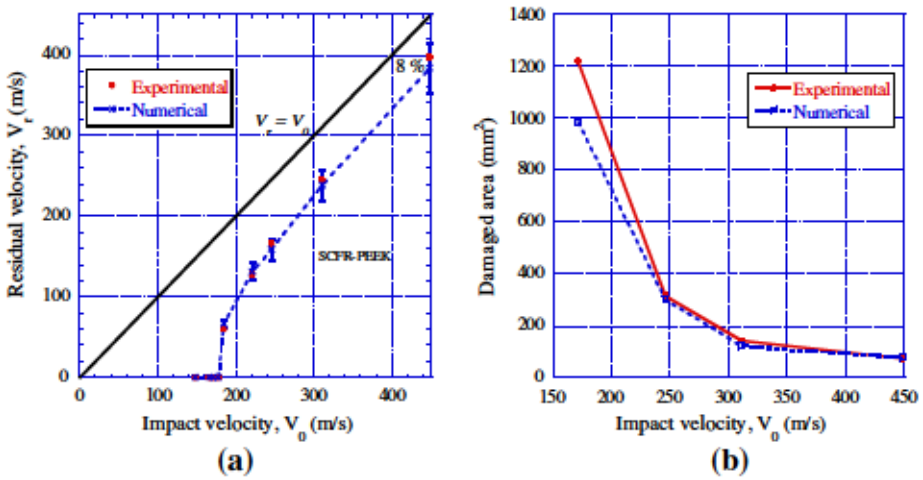

Fig. 16. Experimental and numerical data for SCFR PEEK composite subjected to mechanical impact: (a) residual velocity (b) damage area.

VUMAT subroutine. The images of impacted laminates obtained by the C-Scan allow measuring the damaged area using an image processor software and hence represent the damaged area vs. the impact velocity, Fig. 16b.

7. Conclusions

In this work, the mechanical impact behavior of SCFR PEEK has been investigated using a combination of experiments and finite element simulations. In the full range of impact kinetic energies considered, from 21 J to 131 J, SCFR PEEK composites showed a brittle failure in line with the behavior studied by other authors in terms of fracture toughness. C-Scan and SEM inspection tests on impacted specimens show that the failure of SCFR PEEK is dependent on material directions, derived of anisotropic material properties due to flow molding manufacturing. To allow adequate prediction of failure, an approach for modeling the behavior of SCFR PEEK composites has been proposed which includes homogenization of elastic material and anisotropic damage. The results show good agreement and validation of the predictions against experimental data of energy absorption and damage area for short carbon fiber PEEK composite.

In conclusion, the absorption energy capability of SCFR PEEK decreases drastically in comparison with unfilled PEEK. The brittleness of SCFR PEEK will limit the application of this composite in prosthetic devices employed in areas exposed to impact by accidental fall.

Acknowledgements

The researchers of the University Carlos III of Madrid are indebted to the Ministerio de Ciencia e Innovación de España (Project DPI/2011-24068) and to the Ministerio de Economía y Competitividad de España (Project DPI/2014-57989-P) for financial support towards part of this work. The researchers are indebted to LATI Company for PEEK material supplied. The authors express their thanks to Ms Penelope Miller, Mr. Sergio Puerta, Mr. David Pedroche for their technical support.

References

[1] Scholz MS, Blanchfield JP, Bloom LD, Coburn BH, Elkington M, Fuller JD, et al. The use of composite materials in modern orthopaedic medicine and prosthetic devices: a review. Compos Sci Technol 2011;71(16):1791–803.
[2] Lovald S, Kurtz S. Applications of polyetheretherketone in trauma, arthroscopy and cranial defect repair. In: Kurtz S, editor. PEEK biomaterials handbook. William Andrew Elsevier; 2012. p. 243–60.
[3] Green S. Chapter 3 – Compounds and composite materials. In: PEEK biomaterials handbook. William Andrew Elsevier; 2012. p. 23–48.
[4] Rivard CH, Rhalmi S, Coillard C. In vivo biocompatibility testing of peek polymer for a spinal implant system: a study in rabbits. J Biomed Mater Res 2002;62:488–98.
[5] Wang A, Lin R, Stark C, Dumbleton J. Suitability and limitations of carbon fiber reinforced PEEK composites as bearing surfaces for total joint replacements. Wear 1999;724:225–9.
[6] Horak Z, Pokorny D, Fulin P, Slouf M, Jahoda D, Sosna A. Polyetheretherketone (PEEK), part i: prospects for use in orthopaedics and traumatology. Act Ch Ortho Trauma Cechoslovaca 2010;77:463.
[7] Ramsteiner F, Theysohn R. Tensile and impact strengths of unidirectional Short Fiber-Reinf Thermoplast Compos 1979;10:111–9.

[8] Sarausa J, Remiro P. The mechanical behaviour of PEEK short fiber composites. J Mater Sci 1995;30:3501–8.
[9] Kurtz SM, Day J, Ong K. Isoelastic polyaryletheretherketone implants for total joint replacement. In: Kurtz S, editor. PEEK biomaterials handbook. William Andrew Elsevier; 2012. p. 221–42.
[10] Arias A, Rodríguez-Martínez JA, Rusinek A. Numerical simulations of impact behaviour of thin steel plates subjected to cylindrical, conical and hemispherical non-deformable projectiles. Eng Fract Mech 2008;5:1635–56.
[11] Garcia-Gonzalez D, Rodríguez-Millan M, Vaz-Romero A, Arias A. High impact velocity on multi-layered composite of polyether ether ketone and aluminium. Compos Interface 2015. http://dx.doi.org/10.1080/09276440.2015.1051421.
[12] El-Qoubaa Z, Othman R. Characterization and modeling of the strain rate sensitivity of polyetheretherketone's compressive yield stress. Mater Des 2015;66:336–45.
[13] Karger J, Friedrich K. Temperature and strain-rate effects on the fracture toughness of poly (ether ether ketone) and its short glass-fiber reinforced composite. Polymer 1989;27:1753–60.
[14] Kammoun S. Micromechanical modeling of the progressive failure in short glass-fiber reinforced thermoplastics [PhD Thesis]. Université catholique de Louvain; 2011a.
[15] Kammoun S, Doghri I, Adam L, Robert G, Delannay L. First pseudo-grain failure model for inelastic composites with misaligned short fibers. Compos Part A 2011;42:1892–902.
[16] Mouhmid B, Imad A, Benseddiq S, Maazouz A. A study of the mechanical behavior of a glass fibre reinforced polyamide 6,6: experimental investigation. Polym Test 2006;25:544–52.
[17] Molazemhosseini A, Tourani H, Naimi-Jamal M, Khavand A. Nanoindentation and nanoscratching responses of PEEK based hybrid composites reinforced with short carbon fibers and nano-silica. Polym Test 2013;32:525–34.
[18] Chukov D, Stepashkin A, Maksimkin A, Tcherdyntsev V, Kaloshkin S, Kuskov K, et al. Investigation of structure, mechanical and tribological properties of short carbon fiber reinforced UHMWPE-matrix composites. Compos Part B 2015;76:79–88.
[19] Steinberg EL, Rath E, Shlaifer A, Chechik O, Maman E, Salai M. Carbon fiber reinforced PEEK Optima—A composite material biomechanical properties and wear/debris characteristics of CF-PEEK composites for orthopedic trauma implants. J Mech Behav Biomed 2013;17:221–8.
[20] 20. LATI High Performance Thermoplastic. Polyether-ether-ketone material properties, <http://www.lati.com> 2015.
[21] Garcia-Gonzalez D, Rusinek A, Jankowiak T, Arias A. Mechanical impact behavior of polyether–ether–ketone (PEEK). Compos Struct 2015;124:88–99.
[22] Lee DJ. On studies of tensile properties in injection molded short carbon fiber reinforced PEEK composite. KSM J 1996;10:362–71.
[23] Rae P, Brown E, Orler E. The mechanical properties of poly(ether-ether-ketone) (PEEK) with emphasis on the large compressive strain response. Polymer 2007;48:598–615.
[24] Jonas A, Legras R, Issi J. Differential scanning calorimetry and infra-red crystallinity determinations of polyaryl ether ether ketone. Polymer 1991;32:3364–70.
[25] Wang Z, Zhou Y, Mallick P. Effects of temperature and strain rate on the tensile behaviour of short fiber reinforced polyamide-6. Polym Compos 2002;5:858–71.
[26] Sobieraj M, Rimnac C. Fracture, fatigue and noch behavior of PEEK. In: Kurtz S, editor. PEEK biomaterials handbook. William Andrew Elsevier; 2012. p. 61–73.
[27] Borruto A. A new material for hip prosthesis without considerable debris release. Med Eng Phys 2010;32:908–13.
[28] Colón-Emeric C, Pieper C, Grubber J. Correlation of hip fracture with other fracture types: toward a rational composite hip fracture. Bone 2015;81:67–71.
[29] Van den Kroonenberg A, Hayes W, McMahon T. Hip impact velocities and body configurations for voluntary falls from standing height. J Biomech 1996;29:807–11.
[30] Asgharpur Z, Baumgartner D, Willinger R, Graw M, Peldschus S. The validation and application of a finite element human head model for frontal skull fracture analysis. J Mech Behav Biomed 2013;33:16–23.
[31] Monea A, Van Perre G, Baeck K, Delye H, Verschueren P. The relation between mechanical impact parameters and most frequent bicycle related head injuries. J Mech Behav Biomed 2014;33:3–15.
[32] Arias A, Zaera R, Lopez-Puente JL, Navarro C. Numerical modeling of the impact behavior of new particulate-loaded composite materials. Compos Struct 2003;61:151–9.
[33] Kammoun S, Doghri I, Brassart L, Delannay L. Micromechanical modeling of the progressive failure in short glass–fiber reinforced thermoplastics – First Pseudo-Grain Damage model. Compos Part A 2015;73:166–75.
[34] Dano ML, Gendron G, MIR H. Mechanics of damage and degradation in random short glass fiber reinforced composites. J Thermoplast Compos 2002;15(1):169–77.
[35] Dano ML, Gendron G, Maillette F, Bissonnette B. Experimental characterization of damage of random short glass fiber reinforced composites. J Thermoplast Compos 2006;19(1):79–96.
[36] Zhu K, Schmauder S. Prediction of the failure properties of short fiber reinforced composites with metal and polymer matrix. Comput Mater Sci 2003;28(3–4):743–8.
[37] Notta-Cuvier D, Lauro F, Bennani B. An original approach for mechanical modelling of short-fiber reinforced composites with complex distributions of fiber orientation. Compos Part A-Appl S 2014;62:60–6.
[38] Notta-Cuvier D, Lauro F, Bennani B. Modelling of progressive fiber/matrix debonding in short-fiber reinforced composites up to failure. Int J Solids Struct 2015;66:140–50.
[39] Tsukamoto H. A mean-field micromechanical formulation of a nonlinear constitutive equation of a two-phase composite. Comput Mater Sci 2010;50:560–70.
[40] Müller V, Kabel M, Andrä H, Böhlke T. Homogenization of linear elastic properties of short-fiber reinforced composites – a comparison of mean field and voxel-based methods. Int J Solids Struct 2015;67–68:56–70.
[41] Hill R. Theory of mechanical properties of fiber-strengthened materials: I. elastic behavior. J. Mech Phys Solids 1964;12:199–212.
[42] Hashin Z. The elastic moduli of heterogeneous materials. J Appl Mech 1962;29:143–50.
[43] Tucker CL, Liang E. Stiffness predictions for unidirectional short-fiber composites: review and evaluation. Compos Sci Technol 1999;59:655–71.
[44] Kulkarni A, Aswini N, Dandekar CR, Makhe S. Modeling of short fiber reinforced injection moulded composite. In: IOP Conference Mater Sci Eng 2012.
[45] Rubio-López A, Olmedo A, Santiuste C. Modelling impact behavior of all-cellulose composite plates. Comp Struct 2015;122:139–43.
[46] Hibbitt H, Karlsson B, Sorensen P. Abaqus v6.12 documentation—ABAQUS analysis user's manual. Providence (RI): Dassault Systèmes Simulia; 2012.
[47] Rusinek A, Rodríguez-Martínez J, Zaera R, Klepaczko J, Arias A, Sauvelet C. Experimental and numerical study on the perforation process of mild steel sheets subjected to perpendicular impact by hemispherical projectiles. Int J Impact Eng 2009;36(4):565–87.
[48] Zhang G, Scharlb A. Correlation of the tribological behaviors with the mechanical properties of poly-ehter-ether-ketones (PEEKs) with different molecular weights and their fiber filled composites. Wear 2009;266:337–44.
[49] Wang X, Shi J. Validation of Johnson–Cook plasticity and damage model using impact experiment. Int J Impact Eng 2013;60:67–75.
[50] Recht RF, Ipson TW. Ballistic perforation dynamics. J Appl Mech 1963;30:384–90.
[51] Pernas-Sánchez J, Artero-Guerrero JA, Zahr-Viñuela J, Varas D, López-Puente J. Numerical analysis of high velocity impacts on unidirectional laminates. Compos Struct 2014;107:629–34.
[52] Bourmaud A, Ausias G, Lebrun G, Tachon M, Baley C. Observation of the structure of a composite polypropylene/flax and damage mechanisms under stress. Ind Crops Prod 2013;43:225–36.